Type of contribution:
Editorial
▶ Research Paper
Case Study
Review Paper
Scientific Data
Report of Tech. Application

mesi
e-issn. 2798-5245
Mechanical Engineering for Society and Industry
Vol. 5, No. 1 (2025) pp 268-275
https://doi.org/10.31603/mesi.13499

Microstructures and mechanical properties of friction stir dissimilar AA2024-O/AA6061-T6 welded joints at varying tool rotational speeds

Diana Puspita Sumarno, Mochammad Noer Ilman*

Department of Mechanical and Industrial Engineering, Faculty of Engineering, Universitas Gadjah Mada, Yogyakarta, **Indonesia**
✉ ilman_noer@ugm.ac.id

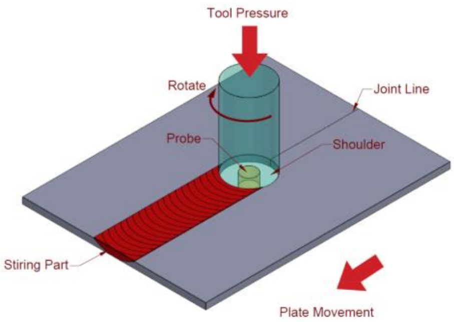

Highlights:

- FSW successfully joined dissimilar AA2024-O and AA6061-T6 at varied tool speeds.
- Higher tool rotation improved metal mixing and microstructural homogeneity in the weld nugget.
- Best tensile strength of around 170.38 MPa was achieved at 1500 rpm due to better homogeneity and precipitation hardening.

Abstract

Friction Stir Welding (FSW) is an innovative solid-state welding technique, especially for joints of unweldable metals or even dissimilar metals. In this study, FSW processes of two dissimilar metals, namely AA2024-O and AA6061-T6, were done at different tool rotational speeds of 910, 1500, and 2280 rpm whilst the welding speed was kept constant at 30 mm/min. This research was intended to improve the mechanical properties of the dissimilar FSW joints. A cylindrical pin-equipped tool was selected, and it was tilted at an angle of 2° during welding. Afterwards, microstructural observations, microhardness, and tensile tests were done. Results demonstrated that increasing tool rotation increased the peak temperature, accompanied by better mixing of different metals in the weld nugget zone (WNZ), hence resulting in improved microstructural homogeneity. The hardness distributions for all dissimilar FSW joints were characterized by the appearance of a high hardness region in the central part of WNZ, resulting in a peak of hardness. It was obtained that the FSW joint at 1500 rpm revealed the best ultimate tensile strength (UTS) around 170.38 MPa, which could be a result of precipitation hardening combined with a better homogeneity in WNZ.

Keywords: Friction stir welding; Dissimilar metals; Tool rotational speed; Strength; Microstructure

Article info
Submitted: 2025-04-05
Revised: 2025-06-03
Accepted: 2025-06-05

Publisher
Universitas Muhammadiyah Magelang

1. Introduction

Aluminum alloys with excellent physical/mechanical properties, such as a high ratio of strength-to-weight, good toughness, good formability, and non-toxic metals, are important engineering materials, especially for lightweight structures. Among high-strength aluminum alloys used as engineering materials, the heat-treatable AA2024-O and AA6061-T6 are the most widely used aluminum alloys. AA2024-O (Al-Cu) and AA6061-T6 (Al-Mg-Si) are frequently used for industrial applications, such as the transportation industry. The copper (Cu) content of AA2024-O aluminium alloy is in the range of 3.8-4.9% whereas O represents annealing to achieve improved ductility [1]. AA2024 and 2XXX series are unweldable by means of traditional fusion welding due to solidification cracking, so that welding such aluminum alloys is challenging [2]. Consequently, a new and innovative welding process, such as friction stir welding (FSW), has been developed to address this issue. On the other hand, AA6061-T6 and its 6XXX series are Al-Mg-Si alloys, which are considered to have good weldability, but weld cracking can occur when magnesium or other elements are added [3].

Welding of dissimilar metals is important, especially for structures that are composed of many components with different materials. The dissimilar metal welding (DMW) is often conducted for two reasons. First, the use of a single metal is more costly, and secondly, to obtain a good combination of mechanical properties and corrosion resistance. Unfortunately, DMW is sometimes done with difficulty due to the significant disparities in the physical, chemical, and metallurgical qualities of the metals to be joined [4]. Recent research works have shown that high-quality welded joints can be fabricated using FSW. FSW is a solid-state welding process in which a welding process is accomplished without melting the metals to be joined, so that solidification cracking can be prevented. FSW is therefore regarded as an efficient joining technique for 6061-T6 and 2024 aluminum alloy welding [5], [6], [7].

To be able to join materials, FSW welding uses a cylindrical tool fitted with a shoulder and a pin, and the formation of joints is aided by the actions of pressure and friction. In this method, the rotating tool is first plunged into a joining line until its shoulder reaches the top surface of the adjoining plates. After that, the rotating tool moves along the weld line, resulting in frictional heat that softens the metals around the tool. Under weld thermal cycle, i.e., heating and cooling rates, several simultaneous thermomechanical processes, including plastic deformation, material flow, and dynamic recrystallization events, are intricately interacting with each other [8], [9]. The material around the pin becomes soft due to the localized frictional heating. Because of tool rotation and translation, the material ahead of the pin flows towards the region behind the pin. As a result, a solid-state joint is created [10]. Additionally, the high-quality FSW joints are determined by many factors such as the type of joint employed, tool rotation speed, tool traveling speed, pin shape, and the angle of tool tilt [11], [12], [13], [14]. Therefore, excellent FSW joints depend on understanding FSW principles and welding parameters.

Over the last decade, research has been conducted extensively to investigate the tool rotation speed effect in dissimilar FSW joints. Amlan *et al*. [15] have researched the effect of tool rotation in the FSW process of dissimilar alloys between Al 2024 and titanium alloy. It was obtained that the tensile properties and weld morphology of the dissimilar metal weld nugget were greatly influenced by the tool rotating speed. Another finding is that the Ti particle fraction was reduced as the rotation speed was raised from 400 to 1200 rpm, and the best UTS and ductility of the dissimilar FSW joints were obtained at 800 rpm. Subsequently, Zhang *et al*. [16], have researched the effects of tool rotation speed on macro- and microstructural features of FSW joints of 6061 aluminum alloy. It was obtained that the tool rotation speed achieved a critical point at 5000 rpm, at which the weld nugget reached an optimal size without any defects formed in the joints. The work of Panwariya & Dwivendi [17] demonstrated that a higher tool rotational speed, typically 1216 rpm, increased strain rate and made the deformation more uniform in the FSW joints of 7075-T651. As a result, a strong B/B texture together with increased dislocation density tended to form in the nugget zone (NZ).

In recent years, there has been a great number of research works on FSW joints of dissimilar metals among various grades of aluminum alloys. Çamet al. [18] have demonstrated an effective solution for joining dissimilar AA6082 and AA2024 using FSW, with the results showing that such a joint could achieve the joint efficiency up to 90%. Subsequently, Ilangovan *et al*. [19] conducted a study on FSW joints of two different metals, namely AA 5086 and heat-treatable AA6061 aluminum alloys with various pin shapes. The results showed that the cylindrical pin with having threaded surface produced the best joint performance. This type of pin produced the weld having smoother precipitate distribution and better material flow, hence making it a superior choice for improving the strength and quality of dissimilar aluminum alloy joints. Although research works on dissimilar FSW joints, different series of aluminum alloys have been extensively conducted; however, the dissimilar FSW joints of AA2024-O and AA6061-T6 with variations in pin shapes have not been reported yet. Thus, it is to be the subject of the current research.

2. Methods

2.1. Materials

In this work, two dissimilar aluminum alloy plates, i.e. AA2024-O and AA6061-T6 were welded using FSW process with their chemistries are given in **Table 1**. The plate dimensions were 300 mm x 100 mm x 3 mm as shown in **Figure 1**a. The tool was made of hardened AISI H13 steel. The tool was designed to have a cylindrical pin with its dimensions were 5 mm in diameter and 2.8 mm in length whereas the tool shoulder diameter was 14 mm as illustrated in **Figure 1**b.

Table 1. Chemical compositions of AA2024-O/AA6061-T6 (wt. %)

Materials	Mg	Si	Cu	Fe	Zn	Ti	Mn	Cr	Others	Al
AA2024-O	1.270	0.970	5.038	0.2569	0.977	0.096	0.452	0.036	Max 0.5	Bal.
AA6061-T6	0.975	0.755	0.242	0.3073	0.016	0.0262	0.070	0.183	Max 0.5	Bal.

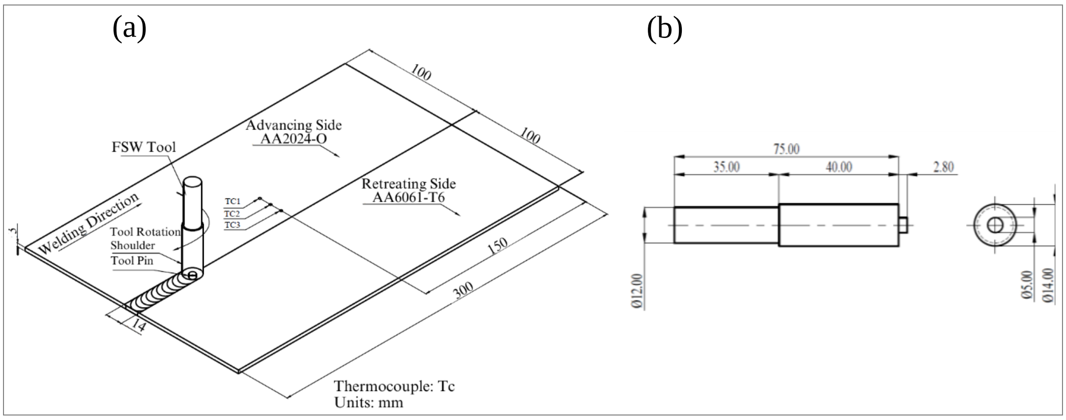

Figure 1. Schematic illustrations of: (a) FSW process and (b) the tool dimensions

2.2. Welding Procedure

The schematic illustration of FSW process at various tool rotating speed is depicted in **Figure 1**a and **Figure 1**b. All FSW processes were done using a tool traveling speed of 30 mm/min. with the tool was tilted at an angle of 2˚ to the vertical axis. The tool rotating speed was varied at 910, 1500, and 2280 rpm. K-type thermocouples (Tc) were employed to record the temperatures of the area near the weld region at the distance of 10, 20 and 30 mm from the joining line. Following the welding process, the positions of specimens extracted from the plates were determined for material characterizations, as illustrated in **Figure 2**.

Microstructural analyses were carried out using a light microscope on the cross-sectional area of the FSW joints according to ASTM E407-99. A sequence of metallographic sample preparation was done including cutting, mounting, grinding using abrasive paper with a grit size of 100-5000, polishing and lastly etching using Keller's reagent. To complete this work, microanalysis studies using SEM incorporated with EDX spectroscopy were done to assess the distributions of elements and various phases in the weld nugget zone.

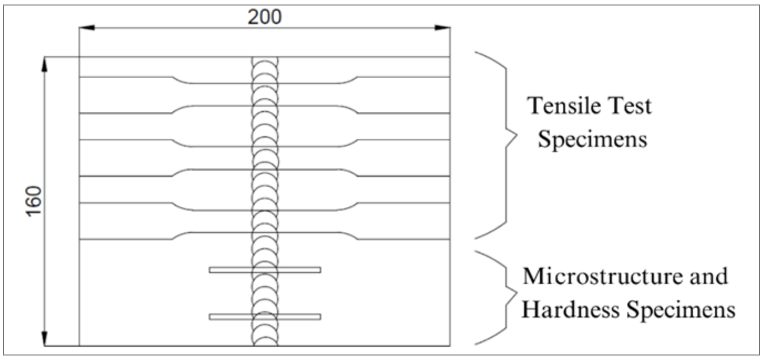

Figure 2. Locations of test specimens

2.3. Hardness measurements

The hardness profiles across various zones of the dissimilar FSW joints were assessed using Vickers microhardness measurements. The hardness data were collected at the mid-thickness of the plates. The measurements were done using a load of 100 gf and a dwell time of 10 s while the point-to-point distance of measurements was 500 mm as shown in **Figure 3**.

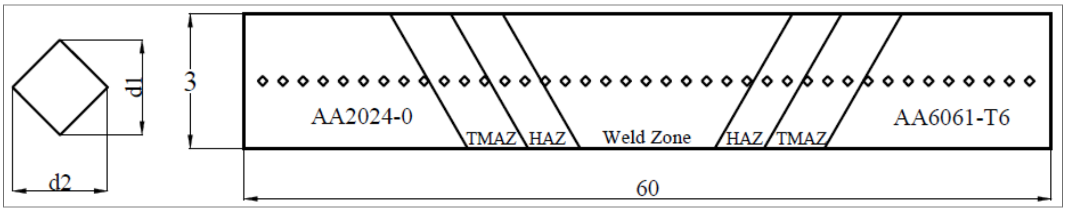

Figure 3. Vickers microhardness specimens

2.4. Tensile tests

As can be seen in **Figure 4**, the tensile test specimens were machined according to ASTM E8 standard. This type of tensile specimen is referred to transverse weld specimen in which the direction of applied load was normal to the weld length direction. The results of these tests included ductility expressed as a percentage of elongation, yield strength (YS), and ultimate tensile strength (UTS). After testing, the fracture surfaces of the specimens were analysed using a light microscope having low magnification.

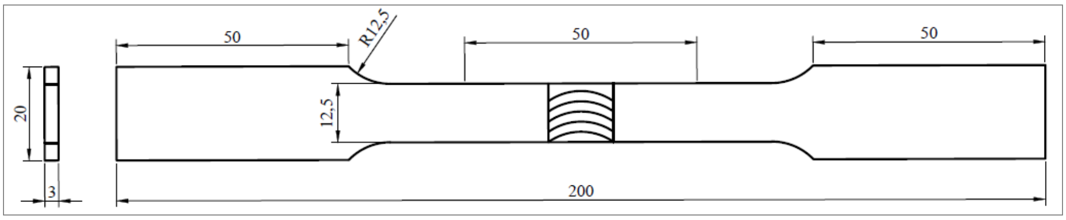

Figure 4.
Tensile test specimens

3. Results and Discussion

3.1. Thermal Cycles in Welding

A study on the welding thermal cycles is of paramount importance since the thermal cycles reflect heating and cooling as the welding process is in progress. Welding deformation, residual stress, microstructure, and hence mechanical characteristics, all of which depend on the weld temperature cycles during FSW [20], [21]. **Figure 5** illustrates the welding thermal cycles at various rotational speeds during FSW, recorded at a distance 10, 20, and 30 mm from the center of weld. The effects of increasing tool rotational speeds are characterized by increasing peak temperature and lowering cooling rate. As the result, the highest peak temperature around 376 °C is resulted by the highest tool rotation speed of 2280 rpm.

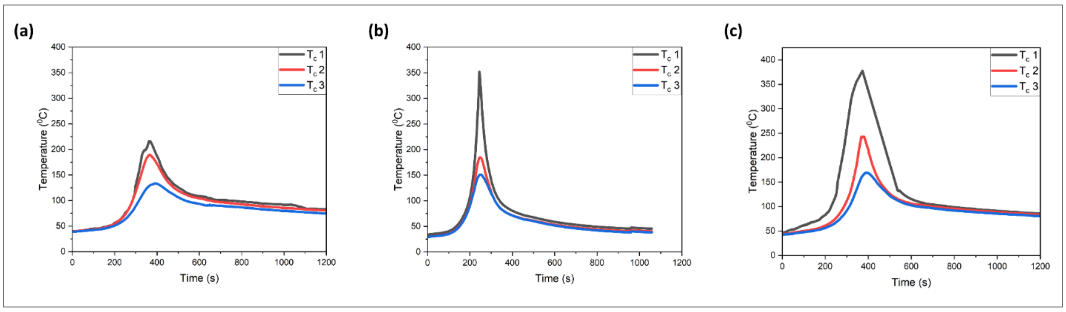

Figure 5.
Weld thermal cycles measured at the tool rotation speeds of: (a) 910 rpm, (b) 1500 rpm, (c) 2280 rpm

The increased peak temperatures at high tool rotation speed can be explained analytically using Eq. (1) [22], where, Q is friction heat, R_{should} is radius of shoulder, R_{pin} is radius of pin, H_{pin} is pin depth, τ_{cont} is shear stress and ω is tool rotation speed.

$$Q = \frac{2}{3}\pi\omega\tau_{cont}(+R^3_{shoul} + 3R^2_{pin}H_{pin}) \tag{1}$$

3.2. Macro and Microstructural Analysis

The macrostructures of FSW joints of dissimilar AA2024-O/AA6061-T6 under various tool rotational speeds are shown in **Figure 6**. Since frictional heat formed in the advancing side (AS) is higher compared to the retreating side (RS), then FSW joints reveal asymmetrically inverted trapezoidal profiles. There are four distinct welding zones, namely base metal (BM), heat-affected zones (HAZ), thermomechanically-affected zones (TMAZ), and weld nugget zones (WNZ). The effects of rotation speeds on the microstructure in WNZ are seen in **Figure 7**a, **Figure 7**b, and **Figure 7**c. At 910 rpm, the WNZ exhibits unmixed regions due to insufficient heat input, while at 1500 rpm, the microstructure morphology changes to fine and equiaxed grains, indicating optimal heat input and efficient recrystallization driven by balanced thermal and mechanical conditions. However, at 2280 rpm, the microstructure shows the evidence of grain coarsening, caused by excessive heat input.

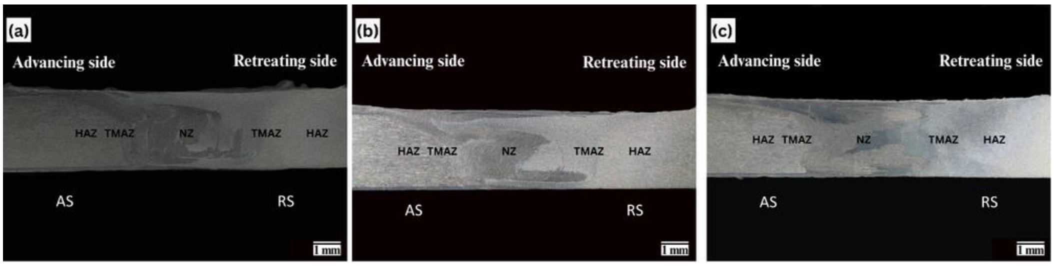

Figure 6. Macrostructure observation in: (a) 910 rpm, (b) 1500 rpm, and (c) 2280 rpm

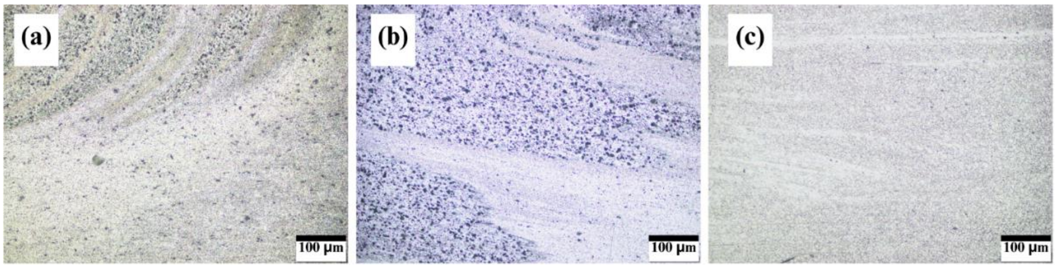

Figure 7. Typical microstructures of FSW AA2024-O/AA6061-T6 at varying rotation speeds at WNZ: (a) 910 rpm, (b) 1500 rpm, and (c) 2280 rpm

Figure 8a shows microstructure of WNZ of the dissimilar FSW joint at tool rotation speed of 1500 rpm using SEM. The EDX spectra taken from two regions, namely region 1 and region 2 **Figure 8**a are shown in **Figure 8**b and **Figure 8**c, respectively. It is seen that the EDX-spectra of region 1 in **Figure 8**a contains high percentage of alloying elements, typically 2.82 wt. % Cu with the small amount of O as shown in Fig. 8(b) suggesting that this region is rich in AA2024-O. In contrast, the region marked 2 in **Figure 8**a consists of 0.77 wt% Mg and 1.00 wt% Si similar to the chemical composition of AA6061-T6.

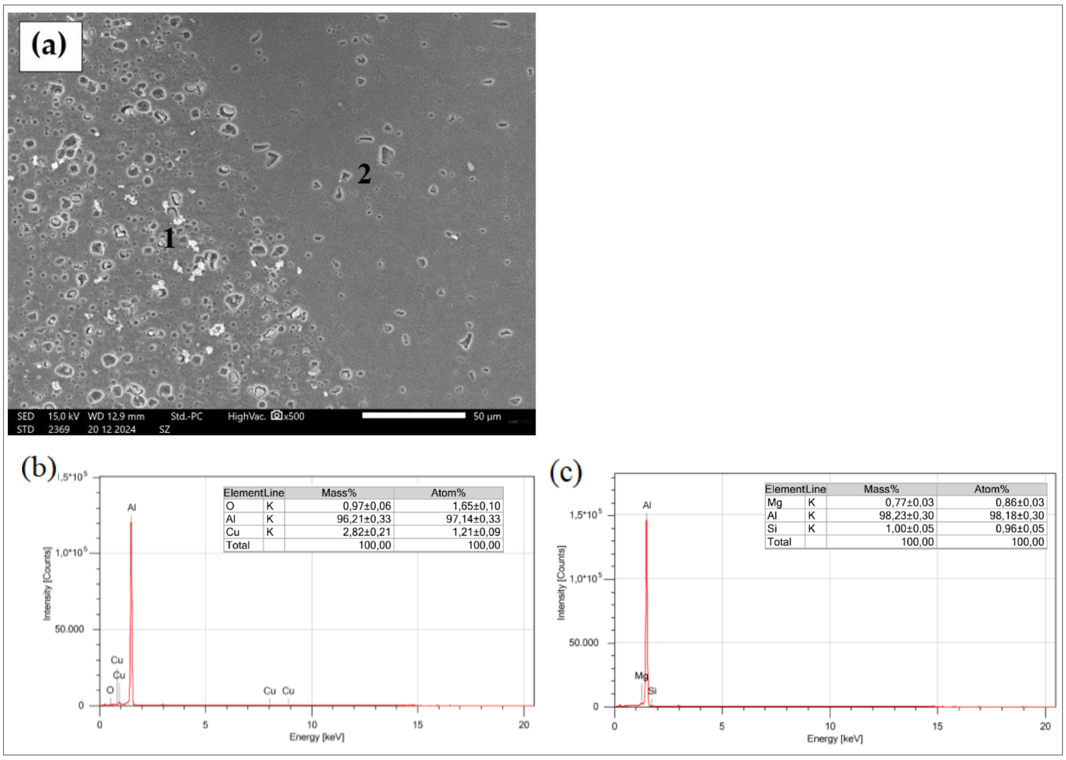

Figure 8. SEM micrograph of WNZ of FSWed dissimilar AA2024-O/AA6061-T6 joint with (b), (c) EDX-spectra of regions marked 1 and 2 in Fig. a

3.3. Microhardness Analysis

Figure 9 shows hardness distributions across various zones of the dissimilar FSW joints at different tool speeds of 910, 1500 and 2280 rpm. The AA2024-O plate has a relatively low hardness around 46.2 Hv. In addition, AA2024-O plate side has a narrow HAZ. This is primarily due to the higher thermal conductivity of AA2024-O which facilitates efficient heat dissipation, hence reducing localized overheating. The rapid heat transfer in AA2024 minimizes microstructural modification in the HAZ. In contrast, the HAZ of the retreating side (AA6061-T6) exhibits a significant drop in hardness because of its lower thermal conductivity compared to AA2024-O [23].

It retains more heat in the HAZ, leading to over aging. Of note is that over aging is characterized by coarsening and dissolution of precipitates, which causes a significant decrease in the hardness. In the WNZ, the hardness significantly increases due to the precipitations of Al2Cu from AA2024-O and Mg2Si from AA6061-T6 which occur in time of welding process.

At a low tool rotation speed (910 rpm), the peak of hardness in WNZ is low due to low friction heat which is not sufficient to promote precipitation. The hardness peaks in the WNZ produce at 1500 rpm are located in the central part of WNZ suggesting that the material flows are optimized. However, at higher rotational speeds (2280 rpm), the peaks of hardness are shifted towards the advancing side (AS). It seems probably that increased heat input and stronger stirring action cause more aggressive material flows, particularly toward the advancing side, leading to a leftward shift in hardness.

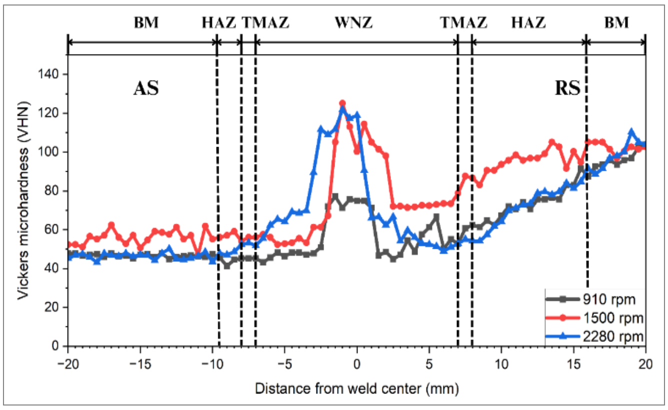

Figure 9. Vickers microhardness profiles of the dissimilar FSW joints at varying tool rotation speeds

3.4. Tensile Test Analysis

Figure 10 shows the results of tensile tests of FSW joints of dissimilar AA2024-O/AA6061-T6 produced by varying rotational speeds (910, 1500 and 2280 rpm). At 910 rpm, the tensile strength and yield strength are 165.11 MPa and 89.11 MPa, respectively, with the elongation of 8.68%. At a higher tool rotation speed of 1500 rpm, the tensile strength reaches its maximum value of 170.38 MPa, along with improved yield strength of 90.72 MPa and elongation of 8.71%. In such a condition, heat input which plasticizes the materias hence material recrystallization and causes precipitation is optimized. However, at 2280 rpm, the tensile strength of 152.76 MPa and yield strength of 91.63 MPa slightly decrease, and elongation drops significantly to 7.52%, likely due to overheating, which causes grain coarsening. Overall, the tool rotation speed of 1500 rpm represents the optimal rotational speed, balancing strength and ductility. Apart from precipitation hardening, the results obtained in this study seem to obey the Hall–Petch [24] principle and it can be explain using Eq. (2), where σ_y is yield strength, σ_o is friction stress and k is locking parameter, and d is grain diameter.

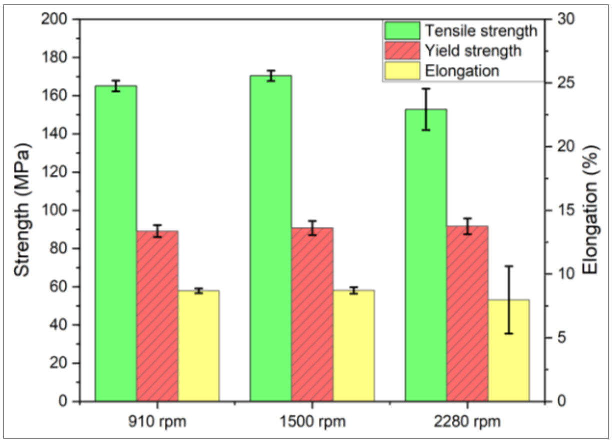

Figure 10. Tensile properties of the dissimilar FSW joints

$$\sigma_y = \sigma_0 + kd^{-1/2} \tag{2}$$

The fracture surfaces of all dissimilar FSW joints after tensile tests are shown in Fig. 11. It is seen that all static fractures are located in AS. It can be seen that the fracture surface of the dissimilar FSW joint at 910 rpm is perpendicular to the applied stress direction, typical of brittle fracture. However, at elevated tool rotation speed, i.e. 1500 rpm or 2280 rpm, the fracture mode changes from tensile to shear mode. In this condition, the orientation of fracture surface forms 45o to the tensile axis. The shear fracture is considered tob ductile fracture.

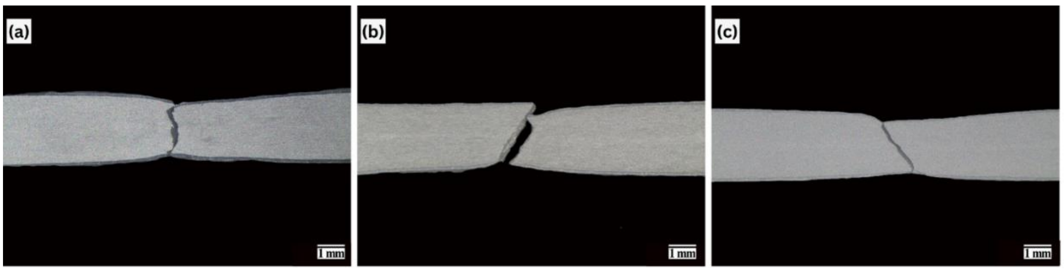

Figure 11. The fracture surfaces after tensile tests showing the location facture in WNZ of AA2024-O advancing side

4. Conclusion

The following conclusions are drawn after conducting several experiments. First, increasing tool rotation speed in FSW process of dissimilar AA2024-O/AA6061-T6 increases the hardness of WNZ but it causes softening in HAZ of AA6061-T6. Secondly, the best tensile strength of the dissimilar FSW joint is obtained at 1500 rpm due to an optimum combination of many factors, especially precipitation and dynamic recrystallization. Finally, the WNZ of FSW joints of dissimilar AA2024-O/AA6061-T6 reveals unmixed region. In this condition, a complete mixing between two different alloys in WNZ can not be achieved.

Acknowledgments

The authors acknowledge the Materials Engineering Laboratory, Universitas Gadjah Mada, for providing the resources needed for this research. We also like to express our gratitude to the Vocational School Laboratory, Universitas Gadjah Mada, for their assistance in conducting the SEM analysis.

Authors' Declaration

Authors' contributions and responsibilities - The authors made substantial contributions to the conception and design of the study. The authors took responsibility for data analysis, interpretation, and discussion of results. The authors read and approved the final manuscript.

Funding – No funding information from the authors.

Availability of data and materials - All data is available from the authors.

Competing interests - The authors declare no competing interests.

Additional information – This article is a selected paper from The 6th Borobudur International Symposium on Science and Technology (6th BIS-STE) 2024. The article has undergone a review process by the scientific committee and was subsequently re-reviewed in accordance with the peer review process of MESI.

References

[1] W. D. Callister and D. G. Rethwisch, *Materials science and engineering: an introduction*, vol. 9. Wiley New York, 2018.

[2] N. Kaushik and S. Singhal, "Experimental investigations on microstructural and mechanical behavior of friction stir welded aluminum matrix composite," *International Journal of Engineering, Transactions A: Basics*, vol. 32, no. 1, pp. 162–170, 2019, doi: 10.5829/ije.2019.32.01a.21.

[3] G. Çam and G. İpekoğlu, "Recent developments in joining of aluminum alloys," *International Journal of Advanced Manufacturing Technology*, vol. 91, no. 5–8, pp. 1851–1866, 2017, doi: 10.1007/s00170-016-9861-0.

[4] L. E. Murr, "A review of FSW research on dissimilar metal and alloy systems," *Journal of Materials Engineering and Performance*, vol. 19, no. 8, pp. 1071–1089, 2010, doi: 10.1007/s11665-010-9598-0.

[5] S. Malopheyev, I. Vysotskiy, V. Kulitskiy, S. Mironov, and R. Kaibyshev, "Optimization of processing-microstructure-properties relationship in friction-stir welded 6061-T6 aluminum alloy," *Materials Science and Engineering: A*, vol. 662, pp. 136–143, 2016, doi: 10.1016/j.msea.2016.03.063.

[6] A. Simar, Y. Bréchet, B. De Meester, A. Denquin, C. Gallais, and T. Pardoen, "Integrated modeling of friction stir welding of 6xxx series Al alloys: Process, microstructure and properties," *Progress in Materials Science*, vol. 57, no. 1, pp. 95–183, 2012, doi: 10.1016/j.pmatsci.2011.05.003.

[7] P. Sadeesh *et al.*, "Studies on friction stir welding of aa 2024 and aa 6061 dissimilar metals," *Procedia Engineering*, vol. 75, pp. 145–149, 2014, doi: 10.1016/j.proeng.2013.11.031.

[8] J. Q. Su, T. W. Nelson, R. Mishra, and M. Mahoney, "Microstructural investigation of friction

stir welded 7050-T651 aluminium," *Acta Materialia*, vol. 51, no. 3, pp. 713–729, 2003, doi: 10.1016/S1359-6454(02)00449-4.

[9] R. Nandan, T. DebRoy, and H. K. D. H. Bhadeshia, "Recent advances in friction-stir welding - Process, weldment structure and properties," *Progress in Materials Science*, vol. 53, no. 6, pp. 980–1023, 2008, doi: 10.1016/j.pmatsci.2008.05.001.

[10] R. S. Mishra and Z. Y. Ma, "Friction stir welding and processing," *Materials Science and Engineering R: Reports*, vol. 50, no. 1–2, pp. 1–78, 2005, doi: 10.1016/j.mser.2005.07.001.

[11] K. K. Kumar, A. Kumar, and S. Sundar, "Investigation of microstructure characteristics and work hardening behaviour of water-cooled FSW dissimilar aluminium alloys," *Materials Today Communications*, vol. 35, no. January, p. 105857, 2023, doi: 10.1016/j.mtcomm.2023.105857.

[12] C. Rathinasuriyan, M. Puviyarasan, R. Sankar, and V. Selvakumar, "Effect of process parameters on weld geometry and mechanical properties in friction stir welding of AA2024 and AA7075 alloys," *Journal of Alloys and Metallurgical Systems*, vol. 7, no. May, p. 100091, 2024, doi: 10.1016/j.jalmes.2024.100091.

[13] M. Zhai, C. S. Wu, and H. Su, "Influence of tool tilt angle on heat transfer and material flow in friction stir welding," *Journal of Manufacturing Processes*, vol. 59, no. July, pp. 98–112, 2020, doi: 10.1016/j.jmapro.2020.09.038.

[14] A. Mamgain, V. Singh, and A. Pratap Singh, "Influence of Welding parameters on Mechanical property during Friction Stir Welded joint on Aluminium Alloys: A Review," *Jurnal Kejuruteraan*, vol. 35, no. 1, pp. 13–28, 2023, doi: 10.17576/jkukm-2023-35(1)-02.

[15] A. Kar, "Effect of Tool Rotational Speed and Mechanisms Associated with Microstructure Evolution and Intermetallics Formation in Friction Stir Welding of Aluminum Alloy to Titanium Alloy," *Journal of Materials Engineering and Performance*, vol. 33, no. 13, pp. 6261–6305, 2024, doi: 10.1007/s11665-023-08407-1.

[16] H. J. Zhang, M. Wang, Z. Zhu, X. Zhang, T. Yu, and Z. Q. Wu, "Nugget Structure Evolution with Rotation Speed for High-Rotation-Speed Friction-Stir-Welded 6061 Aluminum Alloy," *Journal of Materials Engineering and Performance*, vol. 27, no. 3, pp. 1378–1386, 2018, doi: 10.1007/s11665-018-3228-7.

[17] C. Panwariya and D. K. Dwivedi, "Mechanistic insights into abnormal grain growth suppression in friction stir welded 7075-T651 aluminum alloys through variation in tool rotational speed," vol. 40, no. August, 2024.

[18] G. Çam, V. Javaheri, and A. Heidarzadeh, "Advances in FSW and FSSW of dissimilar Al-alloy plates," *Journal of Adhesion Science and Technology*, vol. 37, no. 2, pp. 162–194, 2023, doi: 10.1080/01694243.2022.2028073.

[19] M. Ilangovan, S. Rajendra Boopathy, and V. Balasubramanian, "Effect of tool pin profile on microstructure and tensile properties of friction stir welded dissimilar AA 6061–AA 5086 aluminium alloy joints," *Defence Technology*, vol. 11, no. 2, pp. 174–184, 2015, doi: 10.1016/j.dt.2015.01.004.

[20] Y. Ni, Y. Liu, P. Zhang, J. Huang, and X. Yu, "Thermal cycles, microstructures and mechanical properties of AA7075-T6 ultrathin sheet joints produced by high speed friction stir welding," *Materials Characterization*, vol. 187, no. February, 2022, doi: 10.1016/j.matchar.2022.111873.

[21] L. Buglioni, L. N. Tufaro, and H. G. Svoboda, "Thermal Cycles and Residual Stresses in FSW of Aluminum Alloys: Experimental Measurements and Numerical Models," *Procedia Materials Science*, vol. 9, pp. 87–96, 2015, doi: 10.1016/j.mspro.2015.04.011.

[22] V. A. Karkhin, *Thermal Processes in Welding*. 2019.

[23] V. Drossou-Agakidou *et al.*, "Administration of recombinant human granulocytecolony stimulating factor to septic neonates induces neutrophilia and enhances the neutrophil respiratory burst and β2 integrin expression results of a randomized controlled trial," *European Journal of Pediatrics*, vol. 157, no. 7, pp. 583–588, 1998, doi: 10.1007/s004310050884.

[24] T. Edition, "Physical metallurgy," *Choice Reviews Online*, vol. 43, no. 03, pp. 43-1586-43–1586, 2005, doi: 10.5860/choice.43-1586.